This manuscript is a preprint and has not been peer reviewed. The copyright holder has made the manuscript available under a Creative Commons Attribution 4.0 International (CC BY) license and consented to have it forwarded to EarthArXiv for public posting.

# Multi-Feature Fusion for Grassland Information Extraction and Temporal Change Monitoring

Xiyuan Liu[1#], Jie Chen[1#], Zijin Liu[2#], Xiaohua Zhu[1#], Shigao Jiang[1#], Wanli Kang [1#*]

1. Shaoyang Grassland Resources Protection Center, Shaoyang, Hunan, China;

2. College of Civil Engineering, Xiangtan University, Xiangtan, Hunan, China

*E-mail: 941587169@qq.com (WK)

[#]These authors contributed equally to this work.

## Abstract

Grasslands, as an important terrestrial ecosystem, play a vital role in maintaining ecological security and promoting regional sustainable development. However, in complex mountainous environments, grassland information extraction often suffers from insufficient accuracy, and the underlying mechanisms driving its changes remain unclear. To address these issues, this study takes Chengbu Miao Autonomous County in Hunan Province as the study area. Based on the Google Earth Engine (GEE) platform, a multi-feature fusion framework was constructed by integrating optical imagery, Sentinel-1 SAR data, vegetation indices, texture features, topographic factors, and time-series characteristics. A Random Forest (RF) model was then employed to achieve high-accuracy grassland information extraction. On this basis, multi-year time-series data were utilized to analyze the spatial distribution of grasslands and their interannual variation characteristics. At the county scale, fractional vegetation cover (FVC) was introduced to quantitatively characterize grassland ecological conditions. Furthermore, a typical grassland region, Nanshan Pasture, was selected as a key study area. From both pixel and regional scales, the effects of topographic factors (DEM, slope, and aspect), human activities, and climatic factors (temperature and precipitation) on FVC

This manuscript is a preprint and has not been peer reviewed. The copyright holder has made the manuscript available under a Creative Commons Attribution 4.0 International (CC BY) license and consented to have it forwarded to EarthArXiv for public posting.

were systematically analyzed. The results indicate that multi-feature fusion significantly improves grassland classification accuracy, with optical and SAR data demonstrating strong complementarity under complex surface conditions. The spatial distribution of grasslands in Chengbu County remains generally stable, although localized variations are observed. Grassland area fluctuates between 47.32 and 52.15 km², with relatively small overall changes and no persistent trend of significant expansion or contraction. Meanwhile, FVC values are mainly distributed within the range of 0.59–0.87, exhibiting stage-wise fluctuations, suggesting that grassland ecological conditions remain generally stable but show certain interannual variability. Within the Nanshan Pasture area, FVC shows a significant negative correlation with DEM (r = -0.2839) and a weak negative correlation with human activities (r = -0.1563), while slope and aspect exhibit no significant influence. Among climatic factors, land surface temperature (LST) shows a weak correlation with FVC, whereas precipitation is significantly negatively correlated with FVC (r = -0.589), with its effects primarily acting indirectly through processes such as solar radiation and soil moisture. Overall, grassland vegetation changes in the study area exhibit a pattern characterized by "natural dominance, human regulation, and indirect climatic influence." The multi-feature fusion-based grassland extraction and multi-scale driving factor analysis framework proposed in this study can provide technical support for grassland resource monitoring, ecological assessment, and scientific management in complex terrain regions.

**Keywords：** Multi-feature fusion; grassland resources; Random Forest algorithm; fractional vegetation cover (FVC); spatiotemporal variation

# 1 Introduction

Grasslands are an essential component of terrestrial ecosystems, playing an

This manuscript is a preprint and has not been peer reviewed. The copyright holder has made the manuscript available under a Creative Commons Attribution 4.0 International (CC BY) license and consented to have it forwarded to EarthArXiv for public posting.

irreplaceable role in maintaining ecological security patterns, regulating regional climate, conserving soil and water, and sustaining biodiversity[1, 2]. As an important ecological transitional type linking forests and croplands, grasslands play a crucial regulatory role in carbon cycling, energy exchange, and material transport processes[3, 4]. Meanwhile, grassland resources constitute the material foundation for the development of animal husbandry, and their spatial distribution and quality conditions are directly linked to regional ecological stability and sustainable socio-economic development[5]. However, under the combined influences of climate change and human activities, issues such as grassland degradation, fragmentation, and changes in utilization patterns have become increasingly prominent. This underscores the urgent need for accurate and continuous monitoring of grassland spatial patterns and their temporal dynamics using scientific approaches[6, 7].

With the deepening understanding of grassland ecological functions and their dynamic changes, achieving high-accuracy, long-term time-series monitoring of grassland information has become a key research topic in the fields of ecology and resource management[8]. Traditional field survey methods are constrained by high labor costs, limited spatial coverage, and insufficient temporal efficiency, making it difficult to meet the practical demands of large-scale and continuous monitoring. In contrast, remote sensing technology, with its advantages of synoptic coverage, periodic observation, and repeatability, provides an effective means for identifying grassland spatial distribution and monitoring their dynamic changes[9, 10]. In regions such as Hunan Province, characterized by complex terrain and diverse ecosystems, the monitoring and management of grassland resources have received increasing attention from both governmental authorities and the scientific community. Relevant provincial policies emphasize the establishment of an integrated air–space–ground grassland survey and dynamic monitoring system, along with standardized grassland resource database construction and annual monitoring and evaluation mechanisms, aiming to clarify baseline resource conditions and support ecological protection and utilization decisions. In scientific practice, the integration of multi-source remote sensing data has been widely applied to estimate key ecological indicators, such as biomass, in typical grasslands of Hunan Province, demonstrating significant potential for improving accuracy. However, existing studies have largely focused on data-source synergy or the

This manuscript is a preprint and has not been peer reviewed. The copyright holder has made the manuscript available under a Creative Commons Attribution 4.0 International (CC BY) license and consented to have it forwarded to EarthArXiv for public posting.

application of individual features, and there remains a lack of systematic multi-feature fusion approaches tailored to grassland heterogeneity, as well as long-term time-series change models. Consequently, the complex characteristics of grasslands in terms of spatial patterns, temporal dynamics, and ecological processes have yet to be comprehensively characterized[11, 12].

Overall, although notable progress has been made in remote sensing-based grassland monitoring, it still faces numerous challenges under complex surface conditions. This is particularly evident in regions such as Hunan Province, where hilly and mountainous terrains dominate, land cover types are highly fragmented, and grassland types are diverse[13], Grasslands exhibit pronounced heterogeneity in spectral responses, spatial structure, and seasonal variation characteristics, making it difficult for a single feature or a single data source to achieve stable and accurate grassland information extraction[14]. Meanwhile, existing studies are predominantly based on single-date or short-term analyses, with insufficient attention paid to the long-term evolution processes and temporal dynamics of grasslands. This limitation constrains in-depth investigations into grassland dynamic monitoring and the underlying mechanisms of change[15]. Therefore, it is imperative to develop an integrated methodological framework that incorporates multi-source remote sensing features while jointly accounting for the spectral, structural, and temporal characteristics of grasslands. Such an approach is expected to improve the accuracy of grassland information extraction and enable refined monitoring of grassland spatiotemporal dynamics at the regional scale, thereby providing reliable data support for grassland resource conservation and scientific management in Hunan Province.

Building upon the aforementioned background, this study focuses on complex grassland types encompassing both natural and cultivated grasslands. A multidimensional feature set is constructed by integrating optical data, SAR data, vegetation indices, structural and textural features, topographic variables, and time-series characteristics. Machine learning algorithms, such as Random Forest (RF), are then employed to achieve automated grassland information extraction. Meanwhile, multi-year Sentinel-1 and Landsat time-series data available on the Google Earth Engine (GEE) platform are utilized to monitor grassland changes, with analyses focusing on interannual differences and trend characteristics. On this basis, fractional

This manuscript is a preprint and has not been peer reviewed. The copyright holder has made the manuscript available under a Creative Commons Attribution 4.0 International (CC BY) license and consented to have it forwarded to EarthArXiv for public posting.

vegetation cover (FVC) is introduced as a key indicator for characterizing grassland ecological conditions, enabling quantitative assessment of vegetation growth status. Furthermore, correlation analyses are conducted by incorporating topographic factors (e.g., DEM, slope, and aspect), human activity intensity, and climatic variables (temperature and precipitation), thereby exploring the driving mechanisms of grassland cover changes from a multi-scale perspective. By comprehensively examining the effects of different factors on FVC, this study further elucidates the roles of natural environmental conditions and anthropogenic disturbances in shaping grassland ecosystem dynamics. This study not only evaluates the effectiveness of multi-feature fusion in improving grassland classification accuracy, but also investigates the sensitivity and complementarity of SAR and optical time-series features in grassland dynamic monitoring. Furthermore, an efficient and transferable framework for grassland time-series monitoring is established, providing a scientific basis for grassland resource assessment, ecological conservation, and policy-making.

# 2 Study Area and Data Sources

## 2.1 Overview of the Study Area

Chengbu Miao Autonomous County, administered under Shaoyang City, is located in the western border region of Hunan Province (Fig 1). It lies approximately between 109°58′–110°37′ E and 25°58′–26°42′ N. The elevation ranges from 400 to 2023 m, with an average elevation of nearly 700 m, and a total area of about 2647.07 km². The region is characterized by a mid-subtropical mountainous climate. Topographically, elevations are higher in the southeast and northwest, while the central and northeastern parts are relatively lower, exhibiting highly pronounced terrain variability.

This manuscript is a preprint and has not been peer reviewed. The copyright holder has made the manuscript available under a Creative Commons Attribution 4.0 International (CC BY) license and consented to have it forwarded to EarthArXiv for public posting.

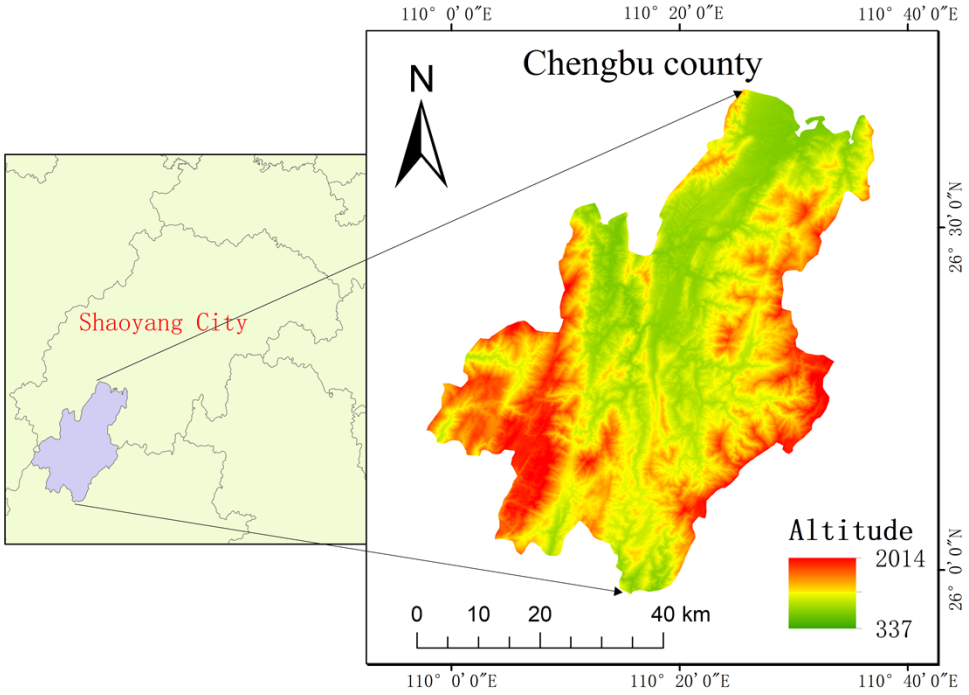


**Fig 1.** Overview of the Study Area

The mid-subtropical mountainous climate of Chengbu provides abundant heat and moisture, endowing vegetation with high productivity potential. Meanwhile, the mid- to high-elevation zones constrain the growth of tall trees, thereby creating favorable ecological niches for herbaceous plants. In the southwestern part of Chengbu, there exists a large high-elevation plateau—Nanshan. Characterized by a flat and open surface, good drainage conditions, sufficient solar radiation, and the accumulation of soil organic matter, Nanshan offers ideal terrain for the formation of concentrated, high-quality grasslands. Grasslands in Chengbu, particularly the Nanshan Pasture, are the result of the coupled effects of four key factors: high-elevation plateau topography, cool and humid climatic conditions, fertile meadow soils, and localized hydrological conditions.

## 2.2 Data Sources and Preprocessing

(1) Remote Sensing Data

Optical remote sensing imagery, vegetation indices, and texture features we

This manuscript is a preprint and has not been peer reviewed. The copyright holder has made the manuscript available under a Creative Commons Attribution 4.0 International (CC BY) license and consented to have it forwarded to EarthArXiv for public posting.

re derived from Landsat data with a spatial resolution of 30 m, covering the study area from March to September during 2000–2025 on the Google Earth Engine (GEE) platform. The datasets include Landsat 5 MSS/TM and Landsat 8/9 OLI/TIRS (Datasets: LANDSAT/LT05/C02/T1_L2, LANDSAT/LC08/C02/T1_L2, and LANDSAT/LC09/C02/T1_L2, all of which have been preprocessed with atmospheric correction, radiometric calibration, and geometric correction.), which have been preprocessed with atmospheric correction, radiometric calibration, and geometric correction. Additional preprocessing steps, including cloud masking and clipping to the study area, were further applied. Topographic features were obtained from the Shuttle Radar Topography Mission (SRTM) dataset (Datasets: USGS/SRTMGL1_003) with a spatial resolution of 30 m on the GEE platform, followed by clipping to the study area. SAR imagery was acquired from the Sentinel-1 dual-polarization C-band Synthetic Aperture Radar (SAR) dataset (Datasets: COPERNICUS/S1_GRD) with a spatial resolution of 10 m, covering the period from March to September during 2015–2025. The dataset has undergone standard preprocessing, including calibration and orthorectification. Furthermore, terrain correction based on the study area DEM and Refined Lee filtering were applied, followed by clipping. To ensure consistency between optical and SAR data, all datasets were resampled to a unified spatial resolution of 30 m.

(2) Sample Data

By integrating field survey data collected from 2021 to 2024 with high-resolution imagery from Google Earth, and based on Sentinel-2 imagery with a spatial resolution of 10 m, a visual interpretation approach was employed to classify land cover types in the study area into six categories: built-up land, cropland, water bodies, forest, bare land, and grassland. Accordingly, a corresponding land cover sample dataset was constructed. The sample data were subsequently converted into raster format and resampled to a unified spatial resolution of 30 m. The dataset was then randomly divided into a training set (65%) and a validation set (35%).

(3) Climate Data

Climate data were obtained from the CHIRPS daily precipitation dataset and the

This manuscript is a preprint and has not been peer reviewed. The copyright holder has made the manuscript available under a Creative Commons Attribution 4.0 International (CC BY) license and consented to have it forwarded to EarthArXiv for public posting.

MODIS land surface temperature (LST) product available on the Google Earth Engine (GEE) platform, with LST used as a proxy for air temperature. The spatial resolution of the precipitation data is approximately 5 km, while the LST data have a spatial resolution of 1 km (Precipitation dataset: UCSB-CHG/CHIRPS/DAILY; LST dataset: MODIS/061/MOD11A2).

(4) Auxiliary Data

Grassland survey data: derived from field measurements.

# 3 Methodology

## 3.1 Overall Technical Workflow

The technical workflow for grassland classification and extraction is illustrated in Fig 2, consisting of two main modules: data acquisition and data processing. Specifically, the workflow includes seven key steps: data preprocessing, feature extraction, sample dataset construction, Random Forest classification, accuracy assessment and comparative analysis, time-series analysis, and correlation analysis. In the data preprocessing stage, optical imagery and texture features are subjected to cloud removal, median compositing, and clipping, while SAR imagery undergoes terrain correction, Refined Lee filtering, and clipping. Feature extraction is conducted based on Landsat-5/8/9 optical imagery, Sentinel-1 SAR data, and DEM, from which optical indices, radar indices, slope, and aspect are derived. During the sample dataset construction stage, sampling regions are delineated according to land cover types, and the samples are divided into training and validation sets. Subsequently, the Random Forest algorithm is employed to perform land cover classification using the training samples and the extracted features. The classification results are then evaluated through accuracy assessment and comparative analysis to verify the effectiveness of the proposed method. Finally, the trained Random Forest model is applied to classify data from 2015 to 2025, generating annual land cover maps and grassland-specific extraction results. Based on these outputs, time-series change characteristics and correlation analyses are further conducted.

This manuscript is a preprint and has not been peer reviewed. The copyright holder has made the manuscript available under a Creative Commons Attribution 4.0 International (CC BY) license and consented to have it forwarded to EarthArXiv for public posting.

## 2.2 Feature Extraction and Construction

In this study, five categories of features were extracted, including original spectral features, vegetation index features, SAR features, topographic features, and texture features, as summarized in Table 2. The original spectral features consist of Landsat bands B1–B7. For vegetation index features, the enhanced vegetation index (EVI), normalized difference vegetation index (NDVI), normalized difference water index (NDWI), modified normalized difference water index (MNDWI), and soil-adjusted vegetation index (SAVI) were selected. SAR features were derived from Sentinel-1 dual-polarization data, including VV and VH backscatter coefficients. Additional SAR-derived features include the ratio vegetation index (RVI), VH/VV ratio, VH–VV difference in dB, and the dual-polarimetric radar vegetation index (DpRVI). Topographic features include the digital elevation model (DEM), slope, and aspect. Texture features were calculated based on gray-level co-occurrence matrix (GLCM) metrics, including angular second moment (ASM), contrast, correlation, dissimilarity, entropy, homogeneity, and variance.

This manuscript is a preprint and has not been peer reviewed. The copyright holder has made the manuscript available under a Creative Commons Attribution 4.0 International (CC BY) license and consented to have it forwarded to EarthArXiv for public posting.

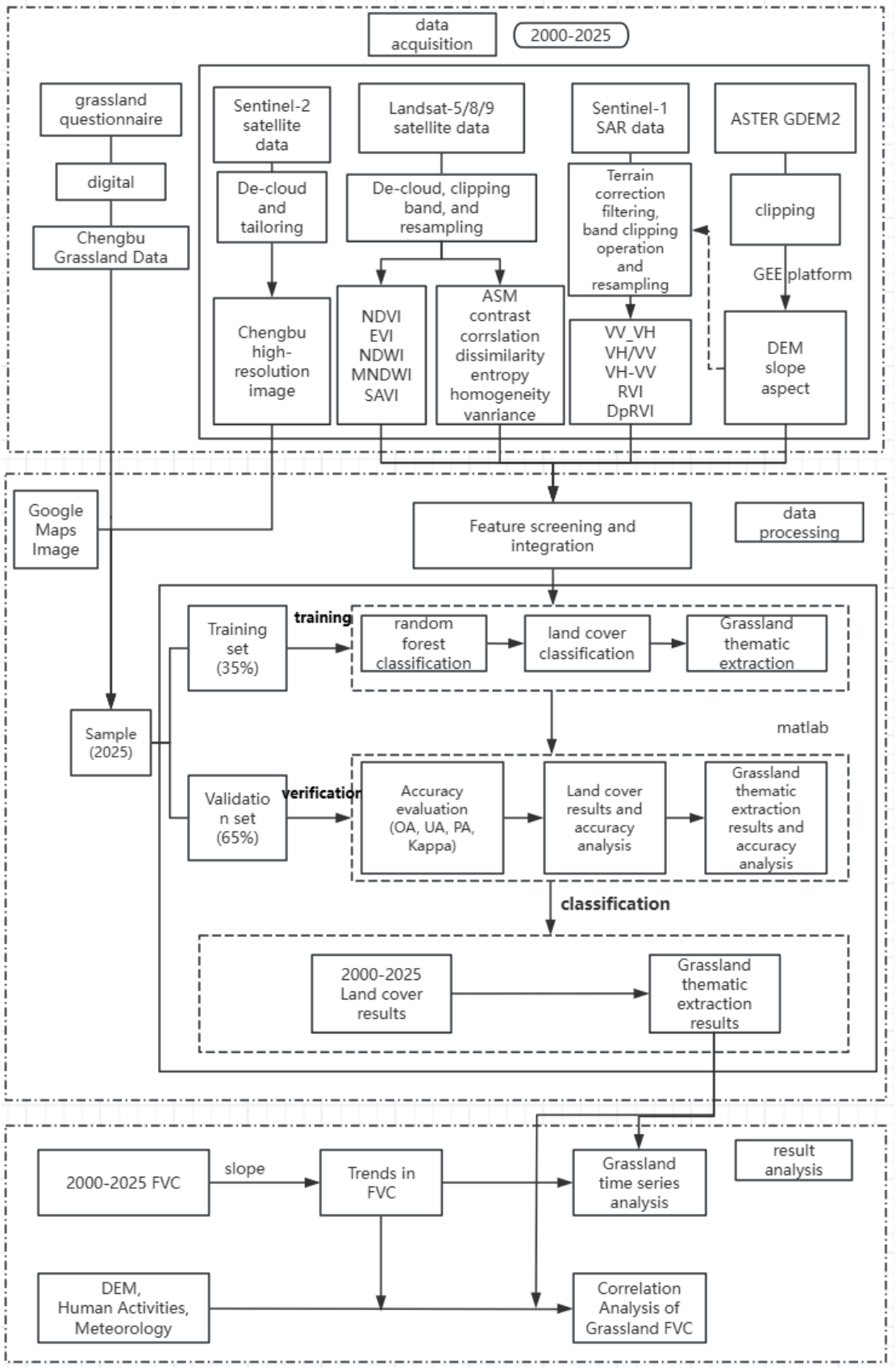


230

This manuscript is a preprint and has not been peer reviewed. The copyright holder has made the manuscript available under a Creative Commons Attribution 4.0 International (CC BY) license and consented to have it forwarded to EarthArXiv for public posting.

231 **Fig 2.** Research Workflow

232 **Table 1. Description of Features**

| Feature Type | Spectral Band Information and Formulas | Note |
|---|---|---|
| Original Spectral Features | B1、B2、B3、B4、B5、B6、B7 | - |
| Optical Index Features | $\mathrm{NDVI} = \frac{\mathrm{NIR} - RED}{NIR + RED}$ | RED: red band; NIR: near-infrared band |
| | $EVI = 2.5 \times \frac{NIR - RED}{NIR - 6 \times RED - 7.5 \times BLUE + 1}$ | BLUE: blue band |
| | $NDWI = \frac{GREEN - NIR}{GREEN + NIR}$ | GREEN: green band |
| | $MNDWI = \frac{GREEN - SWIR}{GREEN + SWIR}$ | SWIR: shortwave infrared band |
| | $SAVI = \frac{NIR - RED}{NIR + RED + \mathrm{L}} \times (1 + \mathrm{L})$ | L: soil adjustment factor (set to 0.5 in this study) |
| SAR Features | VV、VH | VV: co-polarization (vertical transmit, vertical receive); VH: cross-polarization (vertical transmit, horizontal receive) |
| | $R = \frac{\sigma^0\_VH}{\sigma^0\_VV}$ | $\sigma^0$_VH : backscatter coefficient (VH polarization) |
| | $\mathrm{RVI} = \frac{4 \times \sigma^0\_VV}{\sigma^0\_VV + \sigma^0\_VH}$ | $\sigma^0$_VV : backscatter coefficient (VV polarization) |
| SAR Features | $\mathrm{DpRVI} = \left(1 - \frac{\alpha}{\alpha + 1}\right) \times 2, where\ \alpha = \frac{\sigma^0\_VV}{\sigma^0\_VH}$ | $\sigma^0$_VH_dB: backscatter coefficient in decibel (dB) scale for vertical transmit–horizontal receive polarization |
| | $\Delta_{VH-VV} = \sigma^0\_VH\_dB - \sigma^0\_VV\_dB$ | $\sigma^0$_VV_dB: backscatter coefficient in decibel (dB) scale for vertical transmit–vertical receive polarization |
| Topographic Features | DEM、slope、aspect | DEM: Digital Elevation Model; slope: terrain slope; aspect: terrain aspect |
| Texture Features (GLCM-based) | ASM、contrast、correlation、dissimilarity、entropy、homogeneity、variance | ASM: Angular Second Moment |

This manuscript is a preprint and has not been peer reviewed. The copyright holder has made the manuscript available under a Creative Commons Attribution 4.0 International (CC BY) license and consented to have it forwarded to EarthArXiv for public posting.

## 3.3 Feature Importance Analysis and Feature Combination Scheme

Feature importance analysis helps to interpret the decision-making logic underlying "black-box" models, identify less informative features, simplify the model, accelerate training, and provide guidance for model construction. In this study, the out-of-bag (OOB) permutation importance method of the Random Forest (RF) model was employed to quantify the importance of each feature. Based on the resulting importance scores, feature selection was subsequently performed[16, 17]. In this study, different feature sets were used to train the Random Forest (RF) model, and a total of 20 feature combination schemes were designed, as listed in Table 3. After training the model with each scheme, feature importance was calculated to evaluate the contribution of different feature types to the classification decision process of the RF classifier. Based on these results, the feature combinations were further adjusted to optimize the performance of the classifier.

**Table 2. Feature Combination Schemes**

| Scheme | Feature Combination | Scheme | Feature Combination |
|---|---|---|---|
| 1 | A | 11 | A、B、D |
| 2 | B | 12 | A、B、E |
| 3 | C | 13 | A、C、D |
| 4 | D | 14 | A、C、E |
| 5 | E | 15 | A、D、E |
| 6 | A、B | 16 | A、B、C、D |
| 7 | A、C | 17 | A、C、D、E |
| 8 | A、D | 18 | A、B、D、E |
| 9 | A、E | 19 | A、B、C、E |
| 10 | A、B、C | 20 | A、B、C、D、E |

**Note:** A, B, C, D, and E represent topographic features, optical index features, texture features, SAR features, and original spectral features, respectively.

This manuscript is a preprint and has not been peer reviewed. The copyright holder has made the manuscript available under a Creative Commons Attribution 4.0 International (CC BY) license and consented to have it forwarded to EarthArXiv for public posting.

## 3.4 Classification Algorithm and Model Construction

Random Forest (RF) is a classification and regression algorithm based on ensemble learning, proposed by Leo Breiman in 2001[18]. It constructs multiple decision trees and aggregates their predictions through voting (for classification tasks) or averaging (for regression tasks), thereby enhancing the model's generalization ability and robustness.

The core idea of Random Forest originates from bootstrap aggregating (Bagging), whereby multiple subsets are randomly sampled with replacement from the original dataset, and each subset is used to train an independent decision tree. During prediction, the outputs of all trees are aggregated through majority voting (for classification) or averaging (for regression) to obtain the final prediction.

Each decision tree in the Random Forest is typically constructed using the Classification and Regression Tree (CART) algorithm, with the Gini impurity used as the splitting criterion.

$$\mathrm{Gini}(t) = 1 - \sum_{k=1}^{K} [p(k|t)]^2 \quad (1)$$

where $p(k \mid t)$ denotes the proportion of samples belonging to class $k$ at node $t$.

At each node split, a subset of *m_try* features (i.e., the number of randomly selected features considered at each split) is randomly sampled from the full feature set, and the optimal split point is determined from this subset.

During the classification stage, for each test sample, the predictions from all decision trees are aggregated through voting, and the class with the highest frequency is selected as the final prediction.

In this study, different feature sets were used to train the Random Forest (RF) model. First, the training dataset, feature variables, and class labels were input, and the model parameters were configured, with the number of decision trees set to 300 and the bootstrap sampling ratio for each tree set to 63.2%. Next, all features were integrated to perform an initial training of the RF classifier, yielding preliminary land cover

This manuscript is a preprint and has not been peer reviewed. The copyright holder has made the manuscript available under a Creative Commons Attribution 4.0 International (CC BY) license and consented to have it forwarded to EarthArXiv for public posting.

classification results and feature importance scores. Based on these results, the model parameters were adjusted, and features with low importance were removed. The model was then retrained for refined classification, with particular emphasis on further distinguishing grassland types. Finally, feature importance and classification accuracy were jointly analyzed to evaluate the contribution of different features in the classification decision process. Based on this analysis, feature combinations were further optimized to enhance the performance of the classifier.

## 3.5 Accuracy Assessment Methods

Accuracy assessment was conducted based on the confusion matrix, from which overall accuracy (OA), producer's accuracy (PA), user's accuracy (UA), and the Kappa coefficient were calculated. The classification results obtained from different feature sets were compared to evaluate the effects of spectral features, SAR features, and their fusion on classification performance.

**Table 3. Description of Accuracy Metrics**

| Metric | Formula | Note |
|---|---|---|
| Overall Accuracy (OA) | $OA = \frac{\sum_{i=1}^{n} x_{ii}}{N}$ | i : class index; N total number of samples; $x_{ii}$ : number of correctly classified samples; n : number of classes |
| Producer's Accuracy (PA) | $PA_i = \frac{x_{ii}}{r_i}$ | $r_i$ total number of reference samples of class i |
| User's Accuracy (UA) | $UA_i = \frac{x_{ii}}{c_i}$ | $c_i$ : total number of predicted samples of class i |
| Kappa Coefficient | $k = \frac{P_o - P_e}{1 - P_e}$,where ,$P_o$=OA,$P_e = \frac{\sum_{i=1}^{n}(r_i \times c_i)}{N^2}$ | Po : observed agreement; $P_e$ : expected agreement by chance |

## 3.6 Time-Series Analysis

To further reveal the temporal variation characteristics of grassland quantity and quality in the study area, the model was trained using the 2025 sample dataset and applied to classify data from 2015 to 2025. After extracting grassland-specific information for each year, fractional vegetation cover (FVC) was introduced as a key

This manuscript is a preprint and has not been peer reviewed. The copyright holder has made the manuscript available under a Creative Commons Attribution 4.0 International (CC BY) license and consented to have it forwarded to EarthArXiv for public posting.

indicator for evaluating grassland quality, and a slope-based trend analysis was conducted on FVC. FVC represents the proportion of ground area covered by the vertical projection of vegetation and is closely related to vegetation growth status, canopy density, and ecological quality. Therefore, it plays an important role in grassland ecological monitoring. In this study, the Raster Calculator in ArcGIS was used to analyze the spatiotemporal variation of FVC from 2015 to 2025 and to determine its dominant temporal trends, thereby estimating the average rate of increase or decrease in vegetation cover over time.

In this study, fractional vegetation cover (FVC) was estimated based on the Pixel Dichotomy Model (PDM), which assumes that each pixel can be represented as a linear combination of a pure vegetation endmember and a pure soil endmember[19]. The fractional vegetation cover (FVC) is calculated as follows:

$$FVC = \frac{NDVI - NDVI_{soil}}{NDVI_{veg} - NDVI_{soil}} \quad (2)$$

where $NDVI_{soil}$ and $NDVI_{veg}$ represent the NDVI values of pure soil and pure vegetation endmembers, respectively. To ensure the robustness of the endmember selection, the percentile-based method was adopted in this study. Specifically, the 5th percentile of NDVI in the study area was used as the soil endmember, while the 95th percentile was used as the vegetation endmember, expressed as follows:

$$NDVI_{soil} = NDVI_{5\%}, NDVI_{veg} = NDVI_{95\%} \quad (3)$$

To ensure the physical validity of the results, FVC values were constrained within the range of 0 to 1:

$$FVC = \min(1, \max(0, FVC)) \quad (4)$$

Equation (5) presents the calculation formula for the slope-based trend analysis[20]:

$$Slope = \frac{n\sum_{i=1}^{n}(i \times FVC_i) - \sum_{i=1}^{n} i \times \sum_{i=1}^{n} FVC_i}{n\sum_{i=1}^{n} i^2 - \left(\sum_{i=1}^{n} i\right)^2} \quad (5)$$

This manuscript is a preprint and has not been peer reviewed. The copyright holder has made the manuscript available under a Creative Commons Attribution 4.0 International (CC BY) license and consented to have it forwarded to EarthArXiv for public posting.

where *Slope* represents the slope of the regression equation for each pixel, $FVC_i$ denotes the fractional vegetation cover in the *i*-th year, and *n* is the total number of years in the study period. When *Slope* > 0, the FVC of the pixel exhibits an increasing trend; when *Slope* = 0, the FVC remains relatively stable; and when *Slope* < 0, the FVC shows a decreasing trend.

Based on the aforementioned methods, a continuous time series of fractional vegetation cover (FVC) data from 2000 to 2025 was obtained. Subsequently, a joint analysis was conducted by integrating grassland extraction results with annual FVC data. Changes in grassland area reflect the expansion and contraction of grassland quantity, while the temporal variation of FVC further characterizes vegetation growth status, canopy density, and the succession dynamics of grassland quality. On this basis, the slope of FVC change was introduced to quantitatively assess the long-term trend of vegetation cover. The direction and magnitude of the slope were used to determine the degree of improvement or degradation in grassland conditions, thereby identifying the direction and intensity of ecological changes across different regions. By integrating grassland area, FVC levels, and their temporal trends, this study establishes a multidimensional monitoring framework for grassland dynamics in the study area from 2000 to 2025, providing a more systematic and reliable scientific basis for grassland ecological conservation, degradation restoration, and resource management.

## 3.7 Correlation Analysis

To quantitatively analyze the correlation and variation characteristics between fractional vegetation cover (FVC) and its influencing factors, both the Pearson correlation coefficient and the Spearman rank correlation coefficient were employed to assess the relationships between variable pairs. Among them, the Pearson correlation coefficient is used to characterize the linear relationship between variables, and its calculation formula is given as follows:

$$r_{xy} = \frac{\sum_{i=1}^{n}(x_i-\bar{x})(y_i-\bar{y})}{\sqrt{\sum_{i=1}^{n}(x_i-\bar{x})^2 \sum_{i=1}^{n}(y_i-\bar{y})^2}} \quad (6)$$

where $x_i$ and $y_i$ represent the values of the two variables at the *i*-th sample,

This manuscript is a preprint and has not been peer reviewed. The copyright holder has made the manuscript available under a Creative Commons Attribution 4.0 International (CC BY) license and consented to have it forwarded to EarthArXiv for public posting.

respectively; $\bar{x}$ and $\bar{y}$ denote the mean values of the variables; $n$ is the number of samples; and $r_{xy}$ is the Pearson correlation coefficient. The value of $r_{xy}$ ranges from −1 to 1, with values closer to 1 in absolute terms indicating a stronger correlation.

To further characterize the monotonic relationship between variables and reduce the influence of outliers, the Spearman rank correlation coefficient was introduced in this study, and its calculation formula is given as follows:

$$\rho = 1 - \frac{6\sum_{i=1}^{n} d_i^2}{n(n^2-1)} \quad (7)$$

where $d_i$ represents the difference between the ranks of the two variables for the $i$-th sample, and $\rho$ denotes the Spearman correlation coefficient, which also ranges from −1 to 1. By combining Pearson and Spearman correlation analyses, the relationships between grassland FVC and its influencing factors can be comprehensively evaluated from both linear and monotonic perspectives.

# 4 Results and Discussion

## 4.1 Grassland Extraction Results and Accuracy Assessment

The land cover classification results based on different feature combination schemes are shown in Fig 3, including six classes: built-up land, cropland, water bodies, forest, bare land, and grassland. Table 4 presents the number of grassland pixels extracted under different feature combinations, while Table 5 summarizes the classification accuracy of land cover and the user's accuracy (UA) and producer's accuracy (PA) for the grassland class under each feature combination scheme.

This manuscript is a preprint and has not been peer reviewed. The copyright holder has made the manuscript available under a Creative Commons Attribution 4.0 International (CC BY) license and consented to have it forwarded to EarthArXiv for public posting.

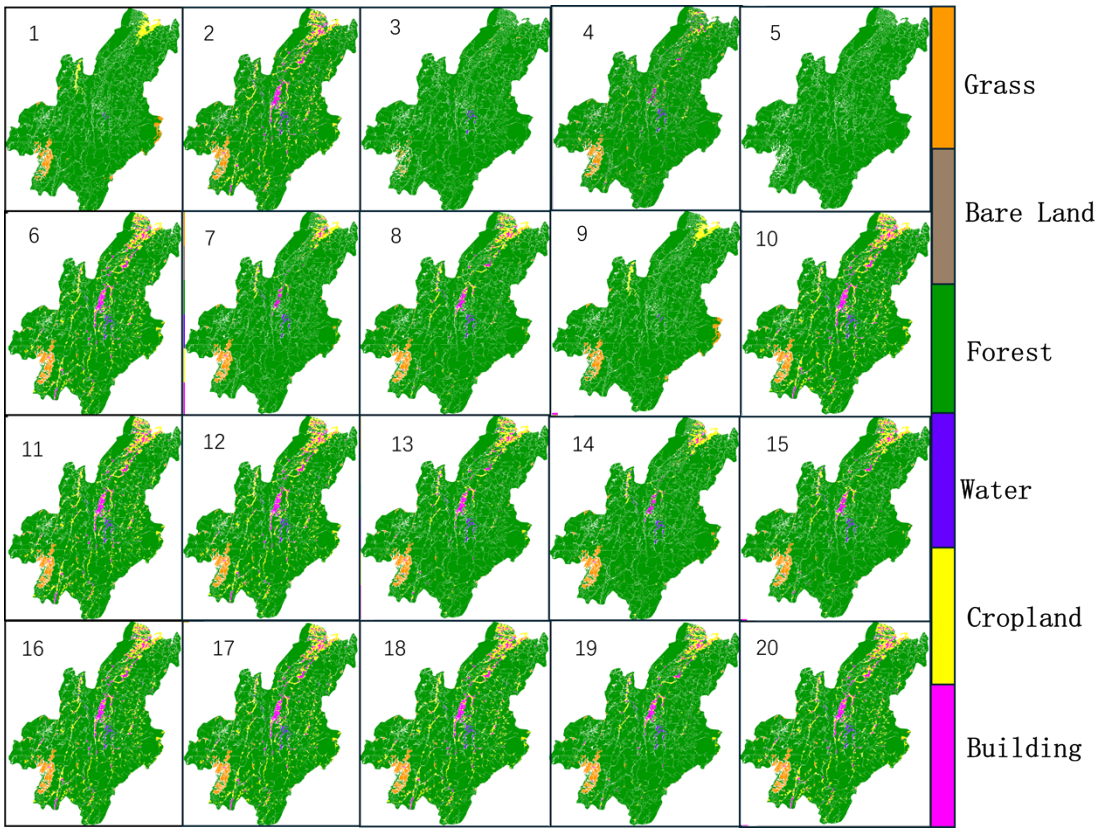


**Fig 3.** Land Cover Types of Chengbu County in 2025 under Different Feature Combination Schemes

From the perspective of grassland extraction quantity (Table 4), among the five single-feature schemes, A, B, C, and D were able to identify a portion of grassland pixels, whereas feature E alone failed to extract any grassland information, resulting in zero detected pixels. In general, multi-feature combinations outperformed single-feature approaches. Among all schemes, Scheme 11 (A, B, C) achieved the highest number of extracted grassland pixels (63,513). Scheme 20 (A, B, C, D, E) yielded 63,431 grassland pixels, which is slightly lower than that of Scheme 11.

**Table 4. Grassland Extraction Results under Different Feature Combination Schemes**

| Scheme | Feature Combination | Number of Grassland Pixels | Area (km²) | Scheme | Feature Combination | Number of Grassland Pixels | Area (km²) |
|---|---|---|---|---|---|---|---|
| Ground Truth | - | 64069 | 51.82 | Ground Truth | - | 64069 | 51.82 |
| 1 | A | 61643 | 49.86 | 11 | A、D | 63513 | 51.37 |

This manuscript is a preprint and has not been peer reviewed. The copyright holder has made the manuscript available under a Creative Commons Attribution 4.0 International (CC BY) license and consented to have it forwarded to EarthArXiv for public posting.

| | | | | | | | |
|---|---|---|---|---|---|---|---|
| 2 | B | 61890 | 50.06 | 12 | ABE | 62576 | 50.61 |
| 3 | C | 15011 | 12.14 | 13 | ACD | 57632 | 46.61 |
| 4 | D | 47407 | 38.34 | 14 | ACE | 61749 | 49.94 |
| 5 | E | 0 | 0 | 15 | ADE | 56539 | 45.73 |
| 6 | AB | 62657 | 50.68 | 16 | ABCD | 63331 | 51.22 |
| 7 | AC | 60896 | 49.25 | 17 | ACDE | 57476 | 46.49 |
| 8 | AD | 56577 | 45.76 | 18 | ABDE | 62708 | 50.72 |
| 9 | AE | 60613 | 49.03 | 19 | ABCE | 62911 | 50.88 |
| 10 | ABC | 62932 | 50.90 | 20 | ABCDE | 63431 | 51.31 |

**Note:** A, B, C, D, and E represent topographic features, optical index features, texture features, SAR features, and original spectral features, respectively.

From the perspective of classification accuracy (Table 5), significant differences are observed among the various feature combination schemes. Among the five single-feature schemes, Scheme 2 (B, i.e., optical index features) achieved the best performance, with an overall accuracy (OA) of 92.74% and a Kappa coefficient of 0.6584. Schemes 1 (A) and 4 (D) showed moderate performance, with OA values of 87.27% and 88.74%, respectively. In contrast, Schemes 3 (C) and 5 (E) exhibited relatively low accuracy, particularly Scheme 5, where the Kappa coefficient is 0, indicating that relying solely on original spectral features is insufficient to effectively distinguish grassland from other land cover types. Among the dual-feature combinations, Scheme 6 (A+B) performed the best, achieving an OA of 93.43% and a Kappa of 0.6976. Although Schemes 8 (A+D) and 7 (A+C) showed improved performance, their accuracies were still lower than that of Scheme 6, suggesting that the combination of optical indices and topographic features is most effective in enhancing grassland separability. For the three-feature combinations, classification accuracy was further improved. Scheme 10 (A+B+C) achieved an OA of 93.67% and a Kappa of 0.7105, while Scheme 11 (A+B+D) reached an OA of 93.58% and a Kappa of 0.7059, both outperforming other three-feature schemes. The complementary effects among A, B, and C are particularly notable. Among the four-feature combinations, Scheme 16 (A+B+C+D) demonstrated strong performance, with an OA of 93.76% and a Kappa of 0.7154, ranking just below the five-feature scheme. The five-feature combination, Scheme 20 (A+B+C+D+E), achieved the highest classification accuracy,

This manuscript is a preprint and has not been peer reviewed. The copyright holder has made the manuscript available under a Creative Commons Attribution 4.0 International (CC BY) license and consented to have it forwarded to EarthArXiv for public posting.

with an OA of 93.79% and a Kappa of 0.7165, making it the best-performing scheme overall. Compared with single-feature schemes, it shows the greatest improvement in OA, indicating that the integration of optical indices, topographic features, texture features, SAR features, and original spectral features maximizes the complementarity of multi-source remote sensing information, thereby significantly enhancing the accuracy and robustness of grassland classification.

**Table 5. Comparison of Land Cover Classification Accuracy under Different Feature Combination Schemes**

| Scheme | Feature Combination | OA/% | Kappa Coefficient | UA/% | PA/% | Scheme | Feature Combination | OA/% | Kappa Coefficient | UA/% | PA/% |
|---|---|---|---|---|---|---|---|---|---|---|---|
| 1 | A | 87.27 | 0.2533 | 56.76 | 58.76 | 11 | ABD | 93.58 | 0.7059 | 93.70 | 94.91 |
| 2 | B | 92.74 | 0.6584 | 89.51 | 93.20 | 12 | ABE | 93.44 | 0.6979 | 92.67 | 95.30 |
| 3 | C | 86.63 | 0.0855 | 21.13 | 97.46 | 13 | ACD | 90.96 | 0.0253 | 85.58 | 96.03 |
| 4 | D | 88.74 | 0.3224 | 69.87 | 96.89 | 14 | ACE | 89.36 | 0.4043 | 80.57 | 83.16 |
| 5 | E | 85.96 | 0 | 0 | 0 | 15 | ADE | 90.73 | 0.5079 | 83.64 | 95.59 |
| 6 | AB | 93.43 | 0.6976 | 92.49 | 94.98 | 16 | ABCD | 93.76 | 0.7154 | 93.76 | 95.19 |
| 7 | AC | 88.13 | 0.4028 | 80.37 | 84.29 | 17 | ACDE | 90.97 | 0.5361 | 85.34 | 96.01 |
| 8 | AD | 90.69 | 0.5053 | 83.65 | 95.70 | 18 | ABDE | 93.53 | 0.7032 | 92.76 | 95.18 |
| 9 | AE | 87.28 | 0.2526 | 56.19 | 59.21 | 19 | ABCE | 93.65 | 0.7093 | 93.32 | 95.37 |
| 10 | ABC | 93.67 | 0.7105 | 93.16 | 95.17 | 20 | ABCDE | 93.79 | 0.7165 | 94.00 | 95.23 |

From the perspective of user's accuracy (UA) and producer's accuracy (PA) for the grassland class, different feature combinations exhibit notable differences in classification reliability and completeness. Among the single-feature schemes, optical index features (Scheme 2, B) not only achieved superior performance in terms of overall accuracy (OA) and Kappa, but also maintained relatively high UA and PA values (UA = 89.51%, PA = 93.20%). This indicates strong discriminative capability for grassland, effectively reducing both commission errors (non-grassland pixels misclassified as grassland) and omission errors (grassland pixels incorrectly excluded). In contrast, Scheme 5 (E), which relies solely on original spectral features, yielded UA and PA values of 0, demonstrating extremely limited capability in distinguishing grassland from other land cover types within the study area, and thus failing to meet

This manuscript is a preprint and has not been peer reviewed. The copyright holder has made the manuscript available under a Creative Commons Attribution 4.0 International (CC BY) license and consented to have it forwarded to EarthArXiv for public posting.

classification requirements. For dual-feature combinations, the integration of optical indices and topographic features (Scheme 6, A+B) significantly improved UA and PA to 92.49% and 94.98%, respectively, compared to single-feature schemes. This suggests that topographic information can mitigate confusion between grassland and other land cover types such as cropland and bare land under complex terrain conditions, thereby enhancing classification reliability. In contrast, combinations without optical index features show relatively limited improvements in UA and PA. For three-feature and higher-order combinations, UA and PA for grassland remain consistently high and stable. In most schemes, PA generally exceeds 95%, while UA is typically above 93%, indicating that multi-source feature fusion not only reduces omission errors but also effectively controls commission errors. In particular, the four-feature combination (Scheme 16, A+B+C+D) and the five-feature combination (Scheme 20, A+B+C+D+E) both achieve optimal UA and PA values. This demonstrates that, with optical index and topographic features as the dominant contributors, the inclusion of texture and SAR features further enriches spatial structural and backscattering information, enabling more robust and stable grassland identification under complex environmental conditions.

The variation patterns of grassland UA and PA are highly consistent with the improvement trends of OA and the Kappa coefficient. However, at the class level, they more intuitively demonstrate the advantages of multi-feature fusion in reducing both commission and omission errors. This further confirms the necessity and effectiveness of integrating multi-source remote sensing features for accurate and refined grassland classification.

## 4.2 Feature Importance Analysis

The feature importance results indicate that different categories of features contribute unequally to grassland classification, with a clear hierarchical structure in their relative importance within the model. Optical remote sensing features and topographic features dominate, serving as the primary sources of information for distinguishing grassland types. Among them, NDVI exhibits the highest importance, significantly exceeding that of other features, highlighting the irreplaceable role of

This manuscript is a preprint and has not been peer reviewed. The copyright holder has made the manuscript available under a Creative Commons Attribution 4.0 International (CC BY) license and consented to have it forwarded to EarthArXiv for public posting.

vegetation indices in characterizing vegetation growth conditions and discriminating grassland from non-grassland classes. DEM ranks second in importance, indicating that terrain variability exerts a strong constraint on the spatial distribution of grasslands, and that topographic conditions play a crucial role in their formation and persistence. In addition, MNDWI and NDWI also show relatively high importance, reflecting the critical role of moisture-related information in grassland extraction, particularly in distinguishing grasslands from similar land cover types such as water bodies and wetlands. Texture features are generally positioned in the third tier of importance, following the primary and secondary feature groups. Among them, homogeneity, differential radar vegetation index (DpRVI), variance, correlation, contrast, and entropy exhibit moderate to relatively high importance. This suggests that texture features effectively complement spectral information by capturing internal structural characteristics and spatial heterogeneity of grasslands. Such features are particularly valuable in areas where spectral similarity among land cover types leads to increased classification confusion. SAR features exhibit lower importance than optical and texture features, ranking fourth overall. Although VV, VH, and their derived features (e.g., VH−VV and VH/VV) contribute to classification to some extent, their importance is relatively low. This indicates that, in the study area, SAR backscattering information has limited sensitivity for grassland identification and primarily serves as an auxiliary enhancement to improve classification performance. This may be attributed to the limited variation in surface roughness within the study area, as well as the relatively weak response of vegetation structure to radar signals[21]. The original spectral band features (B1–B7) exhibit the lowest importance, with some bands showing importance values close to zero. This indicates that single-source raw spectral information is insufficient for effectively distinguishing grassland types, and its discriminative capability is significantly weaker than that of derived index features and texture features. This further highlights the necessity of feature engineering in grassland remote sensing classification. Overall, the analysis reveals that the relative importance of feature categories in grassland extraction follows the order: optical index features and topographic features > texture features > SAR features > original spectral features. This finding provides a basis for subsequent feature optimization and model simplification. It also demonstrates that multi-source feature fusion—particularly approaches dominated by optical indices and topographic information, supplemented by texture

This manuscript is a preprint and has not been peer reviewed. The copyright holder has made the manuscript available under a Creative Commons Attribution 4.0 International (CC BY) license and consented to have it forwarded to EarthArXiv for public posting.

and SAR features—can effectively enhance the accuracy and robustness of grassland classification.

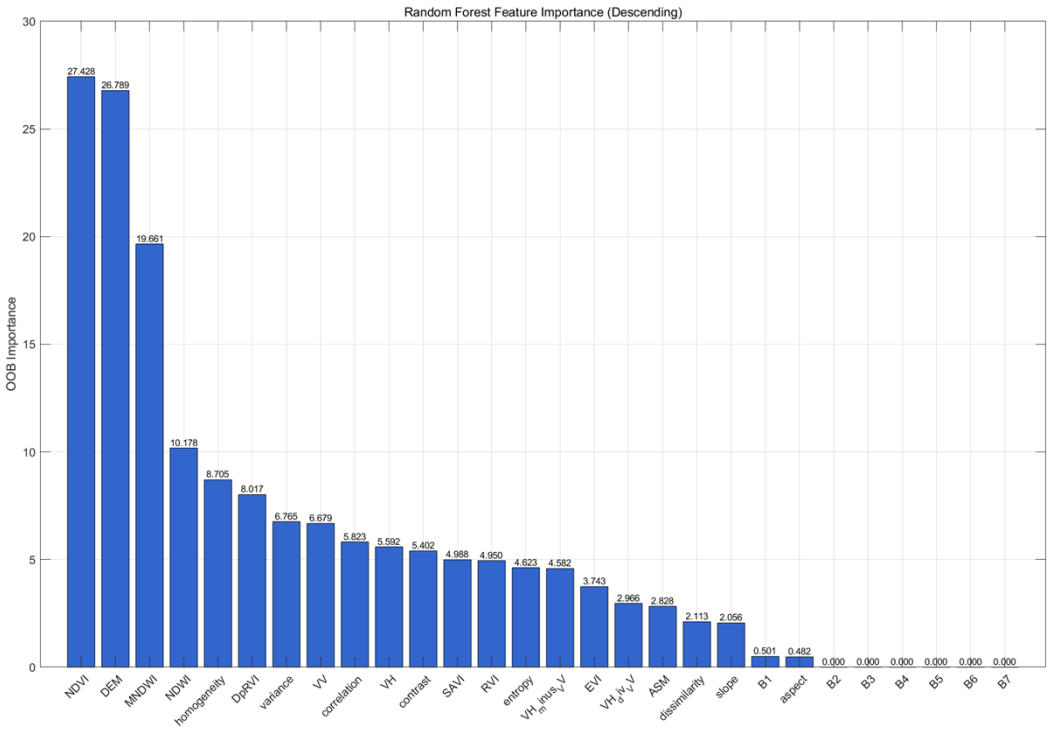


**Fig 4.** Feature Importance

## 4.3 Temporal Analysis of Grassland Changes

Using the Random Forest classification model trained in 2025, land cover classification was performed for the 2015–2025 period based on the five-feature combination dataset, and for the 2000–2011 period using the four-feature combination dataset (without SAR features). The resulting land cover maps from 2000 to 2025 are shown in Figure 5. Grassland area for each year was calculated (Fig 5), and the corresponding fractional vegetation cover (FVC) was derived (Fig 6). The results indicate that over the past 25 years, grassland area exhibits a fluctuating yet overall stable pattern. During the 2000–2011 period, grassland area varied within the range of 47.88–50.79 km². Specifically, it slightly decreased to 47.88 km² in 2003, followed by a notable increase to 50.79 km² in 2005, representing the peak of this period. Subsequently, the area declined slightly and remained relatively stable, fluctuating between 49.7 and 50.5 km² from 2007 to 2011, suggesting no significant expansion or

This manuscript is a preprint and has not been peer reviewed. The copyright holder has made the manuscript available under a Creative Commons Attribution 4.0 International (CC BY) license and consented to have it forwarded to EarthArXiv for public posting.

degradation trend during this stage. In the 2015–2025 period, the fluctuation amplitude of grassland area increased, ranging from 47.32 to 52.15 km². The maximum value of 52.15 km² occurred in 2015, followed by a pronounced decline during 2016–2018, reaching a minimum of 47.32 km² in 2018. Thereafter, grassland area gradually recovered, increasing to 50.44 km² in 2020, declining again to 48.30 km² in 2022, and then showing a recovery trend in 2024–2025, reaching 51.72 km² and 51.31 km², respectively. This pattern indicates a stage-wise fluctuation and recovery in grassland area over the past decade. Overall, although interannual variability exists over the 25-year period, the magnitude of change remains relatively small, with no persistent trend of expansion or contraction. This suggests that grassland resources in the study area have remained generally stable under the combined influence of natural conditions and human activities. However, fluctuations in specific years may be closely related to variations in climatic conditions, land use adjustments, or ecological restoration measures.

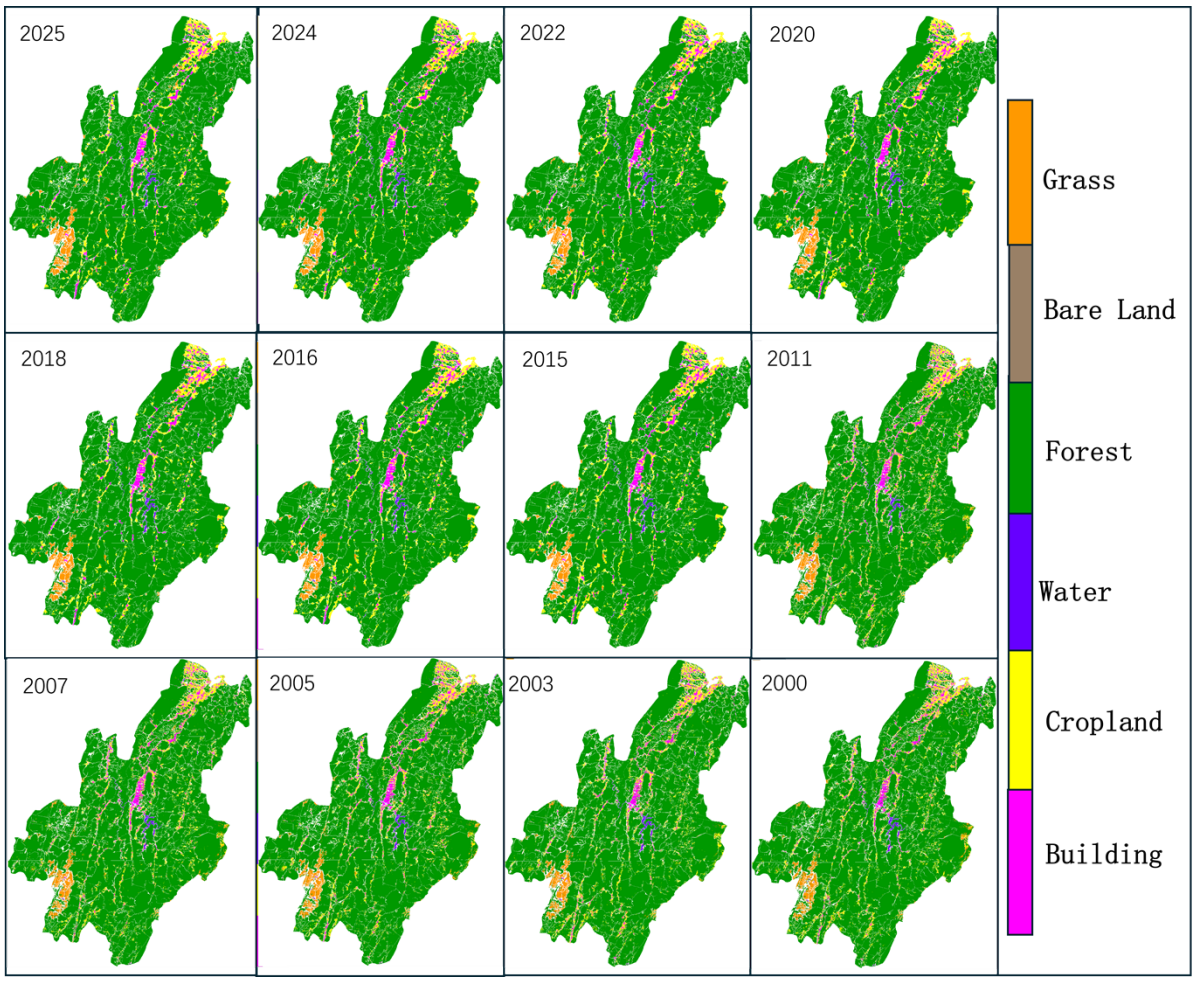

This manuscript is a preprint and has not been peer reviewed. The copyright holder has made the manuscript available under a Creative Commons Attribution 4.0 International (CC BY) license and consented to have it forwarded to EarthArXiv for public posting.

**Fig 5.** Land Cover Types for Each Year

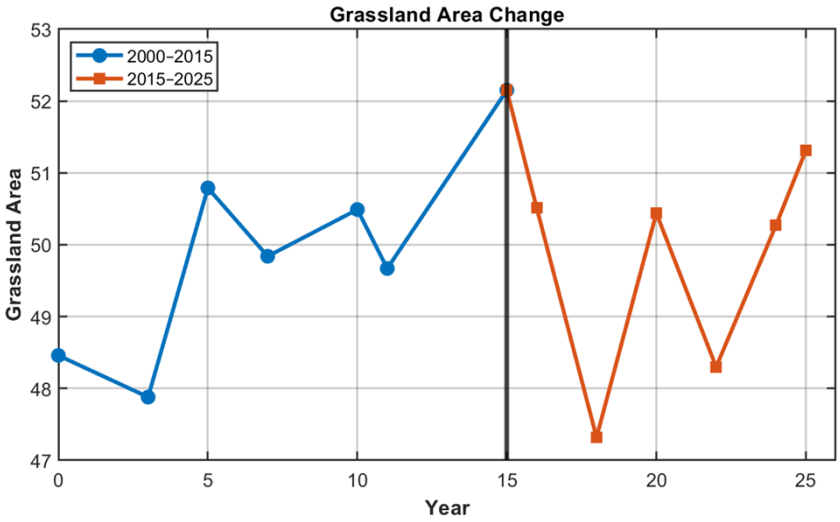


**Fig 6.** Changes in Grassland Area

As shown in Fig 7(a), grassland FVC from 2000 to 2025 exhibits an overall decreasing trend. A pronounced decline is observed during the period 2000–2005, while from 2005 to 2025, FVC shows a fluctuating pattern but remains generally stable. The trends of the mean and median values are largely consistent, indicating a relatively stable variation pattern of vegetation cover in the study area. From the spatial trend shown in Fig 7(b), the grassland area in the southwestern pasture region displays a distinct patchy distribution of FVC changes. Areas with no significant change occupy a large proportion, suggesting that most grassland regions maintained relatively stable vegetation cover during the study period. Meanwhile, localized areas within the pasture exhibit both significant increases and decreases: green patches indicate improvements in vegetation cover and grassland growth conditions, whereas red patches represent declines in FVC, which may be associated with variations in grazing intensity, climatic fluctuations, or localized land use changes.

Overall, the variation in grassland FVC within the study area is dominated by stability, with localized regions exhibiting a coexistence of improvement and degradation. Combined with the temporal analysis, it can be inferred that the overall ecological condition of the main grassland areas remained relatively stable during the study period. However, spatial heterogeneity is evident, as different regions show

This manuscript is a preprint and has not been peer reviewed. The copyright holder has made the manuscript available under a Creative Commons Attribution 4.0 International (CC BY) license and consented to have it forwarded to EarthArXiv for public posting.

varying change patterns under the combined influences of natural conditions and human activities.

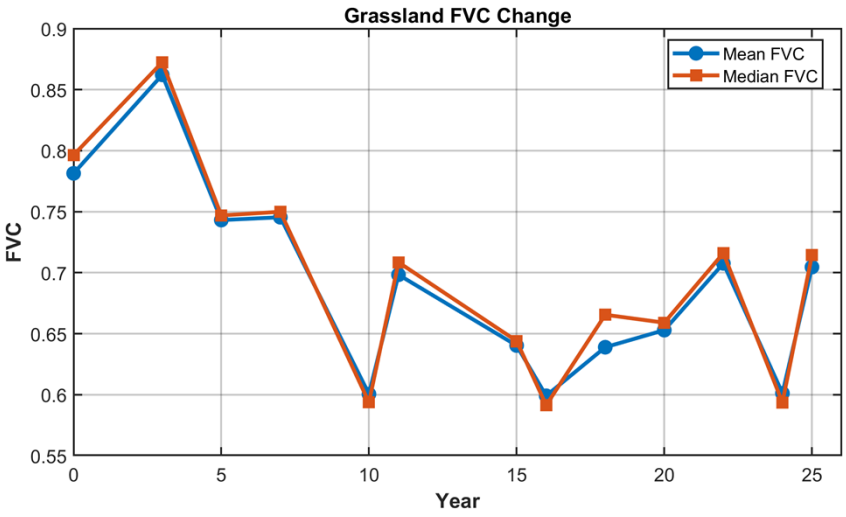


(a) Grassland FVC Changes from 2000 to 2025

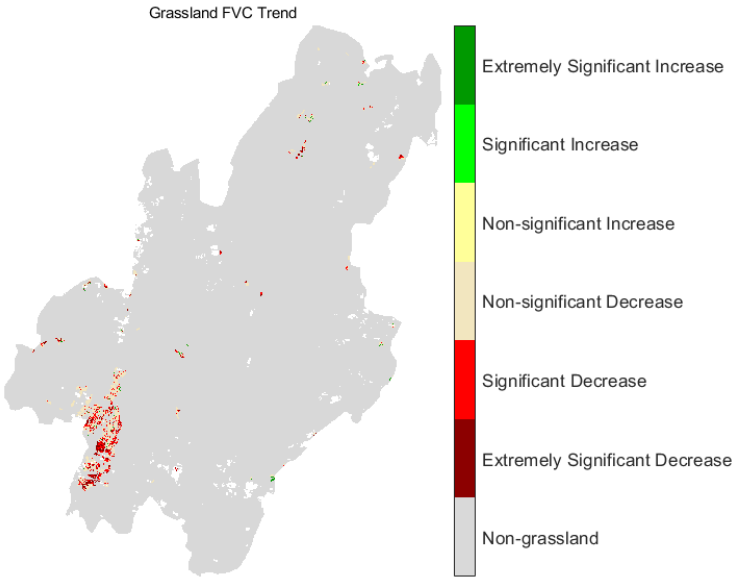


(b) Trend of Grassland FVC from 2000 to 2025

**Fig 7.** Grassland Fractional Vegetation Cover (FVC) and Its Change Trends for Each Year

A combined analysis of grassland area and FVC variations indicates that the overall ecological condition of grasslands in the study area has remained stable. The fluctuations in grassland area and the trends in FVC exhibit a certain degree of consistency during specific periods. For instance, around 2018, both grassland area and

This manuscript is a preprint and has not been peer reviewed. The copyright holder has made the manuscript available under a Creative Commons Attribution 4.0 International (CC BY) license and consented to have it forwarded to EarthArXiv for public posting.

FVC reached relatively low values, suggesting that grassland ecological conditions during this period may have been influenced by climatic factors or human activities. After 2011, although grassland area remained relatively stable, FVC showed a gradual recovery, indicating an improvement in vegetation growth conditions. Overall, grassland resources in the study area have maintained relative stability in terms of quantity, while exhibiting localized fluctuations but overall stability in terms of quality. Vegetation dynamics in the main grassland areas are predominantly stable, with localized regions showing varying degrees of improvement or degradation. This reflects that the grassland ecosystem in the study area exhibits spatial heterogeneity and dynamic change characteristics under the combined influences of natural environmental variations and human activities.

## 4.4 Correlation Analysis

In this study, the Nanshan pasture region was selected as the primary study area. Euclidean distance analysis was performed on human settlements and major roads within the region. The results were then reclassified and subjected to raster calculation and grading to derive a proxy dataset representing human activity intensity. This dataset, together with DEM, slope, and aspect, was used to conduct correlation analysis with grassland FVC in the study area. The results are presented in Table 6 and Fig 8.

The correlation analysis results indicate that, within the grassland areas, fractional vegetation cover (FVC) shows a significant negative correlation with DEM (Pearson $r = -0.2839$, $p < 0.001$). This suggests that FVC generally decreases with increasing elevation. This pattern is primarily attributed to environmental constraints in high-altitude regions, such as lower temperatures and shorter growing seasons. It also reflects the spatial transition of land use types along the elevation gradient in the study area, where forested land gradually shifts toward natural grassland with increasing altitude[22]. Human activity also shows a significant negative correlation with grassland FVC ($r = -0.1563$, $p < 0.001$), although the strength of this relationship is notably weaker than that of DEM. This indicates that human disturbances exert a certain inhibitory effect on vegetation cover, but the overall impact remains relatively limited. This may be attributed to the implementation of grassland protection and ecological

This manuscript is a preprint and has not been peer reviewed. The copyright holder has made the manuscript available under a Creative Commons Attribution 4.0 International (CC BY) license and consented to have it forwarded to EarthArXiv for public posting.

restoration policies in the study area, which have mitigated the negative effects of human activities to some extent. In contrast, the correlation between slope and FVC is not significant ($p > 0.05$), and aspect exhibits only a very weak relationship with FVC ($|r| < 0.05$). These results suggest that micro-topographic factors have a relatively minor influence on grassland vegetation cover in this region. Overall, in the Nanshan pasture area, grassland FVC is primarily controlled by macro-scale natural factors such as elevation, with human activity playing a secondary role, while the effects of slope and aspect are comparatively limited.

**Table 6. Correlation Analysis between Topographic Factors, Human Activities, and Grassland FVC**

| | Pearson | | Spearman | |
|---|---|---|---|---|
| | Correlation (r) | p-value | Correlation (ρ) | p-value |
| DEM | -0.2839 | <0.001 | -0.2700 | <0.001 |
| Slope | 0.0411 | <0.001 | 0.0087 | <0.001 |
| Aspect(sin) | 0.0370 | <0.001 | 0.0402 | <0.001 |
| Aspect(cos) | 0.0402 | <0.001 | 0.0277 | <0.001 |
| Human Activity | -0.1563 | <0.001 | -0.1678 | <0.001 |

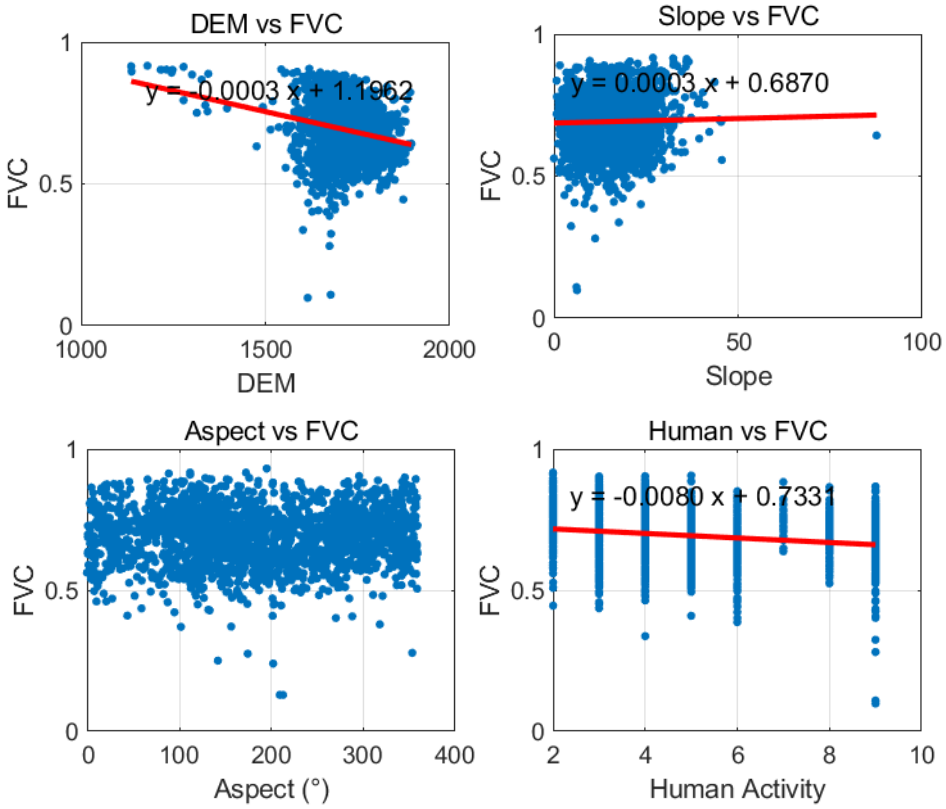

This manuscript is a preprint and has not been peer reviewed. The copyright holder has made the manuscript available under a Creative Commons Attribution 4.0 International (CC BY) license and consented to have it forwarded to EarthArXiv for public posting.

589 **Fig 8.** Correlation Analysis between Topographic Factors, Human Activities, and Grassland FVC

590 Climatic conditions are important driving factors influencing variations in
591 grassland fractional vegetation cover (FVC). In this study, CHIRPS daily precipitation
592 data and MODIS land surface temperature (LST) products were employed, with LST
593 used as a proxy for air temperature. These datasets were selected because their temporal
594 coverage satisfies the requirement for a continuous 25-year study period from 2000 to
595 2025, ensuring the completeness and consistency of the time series. Considering the
596 relatively coarse spatial resolution of meteorological data (approximately 1–5 km),
597 which is insufficient for pixel-scale correlation analysis, this study conducted the
598 analysis at the regional scale. Specifically, monthly climate data during the growing
599 season (March–September) were extracted for each year within the study area. LST was
600 averaged to obtain monthly mean temperature, while precipitation data were first
601 temporally accumulated and then used to calculate monthly mean precipitation.
602 Subsequently, the mean temperature and average monthly precipitation during the
603 growing season were derived. Based on these data, correlation analysis was performed
604 between the climatic factors and the corresponding regional mean FVC of grasslands
605 to evaluate the overall impact of climate variability on vegetation cover. The results are
606 presented in Fig 9.

607 The correlation analysis indicates that grassland fractional vegetation cover (FVC)
608 exhibits a weak positive correlation with land surface temperature ($r = 0.385$), but this
609 relationship is not statistically significant ($p > 0.05$), with a low coefficient of
610 determination ($R^2 = 0.15$). This suggests that LST has limited explanatory power for
611 variations in grassland FVC. Considering the regional context, the Nanshan pasture is
612 located in a humid subtropical climate zone, where thermal conditions are generally
613 sufficient and show limited interannual variability. Therefore, temperature is not a
614 primary limiting factor for vegetation growth, which explains its insignificant influence
615 on FVC dynamics. In contrast, FVC shows a significant negative correlation with
616 precipitation ($r = -0.589$, $p < 0.05$, $R^2 = 0.35$), indicating that precipitation plays a role
617 in influencing grassland cover dynamics. However, this negative relationship does not
618 imply an inhibitory effect of precipitation on vegetation growth. Instead, it is more
619 likely associated with the following factors: (1) Precipitation in the Nanshan pasture is
620 abundant and largely concentrated during the growing season. Frequent rainfall events

This manuscript is a preprint and has not been peer reviewed. The copyright holder has made the manuscript available under a Creative Commons Attribution 4.0 International (CC BY) license and consented to have it forwarded to EarthArXiv for public posting.

are often accompanied by persistent cloud cover and fog, which reduce solar radiation and sunshine duration, thereby limiting photosynthetic activity; (2) Excessive precipitation may lead to elevated soil moisture or even temporary waterlogging, which can restrict root respiration and consequently inhibit vegetation growth; (3) Long-term grazing activities in the study area may also disturb grassland cover, thereby weakening the direct influence of climatic factors.

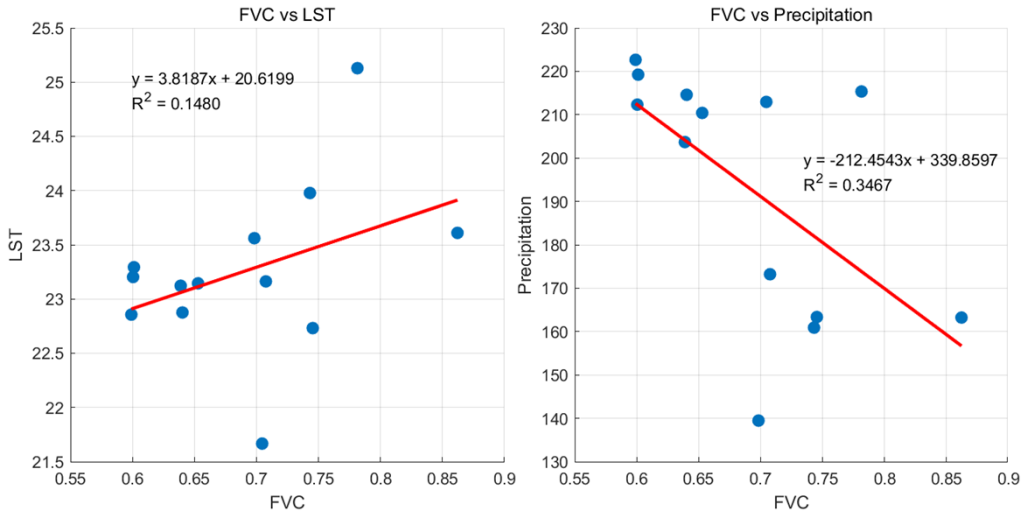


**Fig 9.** Correlation Analysis between Climatic Factors and Grassland FVC

# 5 Conclusions

This study systematically conducted grassland classification accuracy assessment, feature importance analysis, and grassland cover change monitoring from 2015 to 2025 based on multi-source remote sensing feature fusion and a Random Forest model. The main conclusions are as follows:

(1) Among the single-feature schemes, optical index features perform the best; however, they are insufficient to fully distinguish grasslands from cropland, forest, and bare land due to spectral overlap among these land cover types. Overall, multi-feature combinations outperform single-feature approaches. Specifically, the A+B+C scheme (Scheme 11) achieves the best performance in terms of grassland extraction quantity, while the A+B+C+D+E scheme (Scheme 20) attains the highest overall classification accuracy (OA = 93.79%, Kappa = 0.7165). These results demonstrate that optical

This manuscript is a preprint and has not been peer reviewed. The copyright holder has made the manuscript available under a Creative Commons Attribution 4.0 International (CC BY) license and consented to have it forwarded to EarthArXiv for public posting.

indices, original spectral features, topographic features, texture features, and SAR features exhibit strong complementarity, and that multi-source feature fusion can effectively enhance the discriminative capability and robustness of the model under complex surface conditions.

(2) NDVI and DEM exhibit the highest contributions to the model, significantly exceeding those of other features, indicating that vegetation growth status and topographic conditions are the dominant factors controlling grassland classification and FVC estimation. Among all features, vegetation- and moisture-related indices, such as NDVI, MNDWI, and NDWI, rank consistently high, highlighting the critical role of spectral information—particularly indicators reflecting vegetation vigor and surface moisture—in distinguishing grassland types. Texture features (e.g., homogeneity, variance, contrast, and correlation) rank second, demonstrating their importance in characterizing spatial heterogeneity and compensating for spectral similarity among land cover types. In comparison, SAR-related features (e.g., VV, VH, and their combinations) show moderate contributions. Although they are not dominant, they provide auxiliary value by enhancing surface structural information and improving model robustness under complex surface conditions. Overall, the synergistic integration of multi-source features effectively enhances the model's capability to comprehensively represent grassland characteristics, with spectral and topographic factors playing a central role.

(3) The number of grassland pixels in the study area remains generally stable, exhibiting only minor fluctuations without any significant large-scale expansion or contraction. This indicates that, under the combined influence of natural environmental conditions and human activities, the spatial distribution pattern of grasslands has remained relatively stable. Fractional vegetation cover (FVC) shows noticeable interannual variability during 2000–2025, with values ranging approximately from 0.59 to 0.86. Specifically, FVC reached its highest level (approximately 0.86) in 2003, indicating favorable vegetation growth conditions during that period, while it declined to a relatively low value (approximately 0.59) around 2010, reflecting a temporary weakening of vegetation growth. Subsequently, FVC gradually recovered and remained at a moderately high level (0.60–0.70) with slight fluctuations in the later period. Overall, while grassland area exhibits minimal variation, FVC demonstrates fluctuating

This manuscript is a preprint and has not been peer reviewed. The copyright holder has made the manuscript available under a Creative Commons Attribution 4.0 International (CC BY) license and consented to have it forwarded to EarthArXiv for public posting.

673 yet generally stable dynamics, suggesting that the grassland ecosystem in the study area
674 possesses a certain degree of stability and resilience over long-term evolution.
675 Meanwhile, the stage-wise fluctuations in FVC indicate that grassland ecological
676 conditions are still influenced by the combined effects of climate variability,
677 precipitation patterns, and human activity intensity.

678 (4) The integrated correlation analysis of topographic factors, human activities,
679 and climatic variables indicates that the spatial distribution and dynamics of grassland
680 fractional vegetation cover (FVC) in the Nanshan pasture are jointly driven by multiple
681 factors. Among them, elevation (DEM) is the dominant controlling factor, exhibiting a
682 significant negative correlation with FVC, which reflects the influence of climatic
683 constraints and land use differences in high-altitude areas, where vegetation cover tends
684 to be lower. Human activity also shows a significant negative correlation with FVC,
685 although its influence is relatively weak, suggesting that anthropogenic disturbances
686 exert a certain inhibitory effect on grasslands. However, under the implementation of
687 ecological protection and restoration policies, this impact is generally moderated. In
688 contrast, slope and aspect show no significant relationship with FVC, indicating that
689 micro-topographic factors play a limited role. Regarding climatic factors, land surface
690 temperature shows a weak and insignificant correlation with FVC, implying that
691 thermal conditions are not the primary limiting factor. Although precipitation exhibits
692 a significant negative correlation with FVC, its influence is likely indirect, mainly
693 through processes such as reduced solar radiation and altered soil moisture conditions.
694 Overall, grassland FVC in the study area demonstrates a combined control pattern
695 characterized by “natural dominance, human regulation, and indirect climatic influence.”

696 (5) This study achieved grassland information extraction based on multi-feature
697 fusion and a Random Forest model, and further conducted correlation analysis of
698 fractional vegetation cover (FVC) by integrating topographic factors, human activities,
699 and climatic variables. Overall, it provides a relatively robust and interpretable
700 technical framework for grassland classification and the investigation of driving
701 mechanisms. However, several limitations remain. In terms of grassland classification,
702 redundancy may exist among features, and the availability of SAR time-series data is
703 still limited, constraining the fine characterization of grassland dynamics. Regarding
704 the analysis of driving mechanisms, due to the coarse spatial resolution of climatic data,

This manuscript is a preprint and has not been peer reviewed. The copyright holder has made the manuscript available under a Creative Commons Attribution 4.0 International (CC BY) license and consented to have it forwarded to EarthArXiv for public posting.

the analysis was conducted only at the regional scale, which fails to capture pixel-level variability. In addition, the lag effects of climatic factors such as precipitation were not considered, potentially leading to an underestimation of their actual influence. Furthermore, key factors such as grazing intensity, soil properties, and policy regulation were not quantitatively incorporated, which restricts a more comprehensive understanding of grassland change mechanisms. Future research can be extended in several directions. First, higher spatial and temporal resolution remote sensing and meteorological datasets should be incorporated, combined with data fusion techniques to improve analytical accuracy. Second, deep learning methods can be integrated with multi-source features to further enhance grassland classification and change detection performance. Third, multi-factor coupling models should be developed by jointly considering climatic lag effects, human activity intensity, soil properties, and ecological policies, enabling multi-scale integrated analysis. Finally, non-linear modeling approaches (e.g., machine learning or deep learning models) can be explored to more accurately capture the complex driving mechanisms of grassland dynamics in heterogeneous ecosystems.

# Acknowledgments

The authors would like to thank all participants and administrators involved in this study for their support. The authors also acknowledge the use of ChatGPT for English language editing and grammar refinement.

# Author contributions

**Conceptualization:** Xiyuan Liu, Wanli Kang, Xiaohua Zhu.
**Formal analysis:** Zijin Liu, Xiaohua Zhu.
**Funding acquisition:** Xiyuan Liu, Wanli Kang.
**Investigation:** Jie Chen, Shigao Jiang, Zijin Liu.
**Resources:** Jie Chen, Shigao Jiang.
**Supervision:** Xiyuan Liu, Wanli Kang.
**Writing – original draft:** Zijin Liu.
**Writing – review & editing:** Xiyuan Liu, Wanli Kang, Jie Chen.

This manuscript is a preprint and has not been peer reviewed. The copyright holder has made the manuscript available under a Creative Commons Attribution 4.0 International (CC BY) license and consented to have it forwarded to EarthArXiv for public posting.

# References


1. Li T, Cui L, Lv W, Song X, Cui X, Tang LJH. Exploring the frontiers of sustainable livelihoods research within grassland ecosystem: A scientometric analysis. Heliyon. 2022;8(10). doi: 10.1016/J.HELIYON.2022.E10704.

2. Wang P, Shang S, Rong Z, Sun J, Ma J, Lu Z, et al. Unraveling Belowground Community Assembly in Temperate Steppe Ecosystems. Biology. 2025;14(10):1350-. doi: 10.3390/biology14101350.

3. Shan N, Wang T, Zhang Q, Gong J, He M, Zhang X, et al. Monitoring Long-Term Vegetation Dynamics in the Hulun Lake Basin of Northeastern China Through Greening and Browning Speeds from 1982 to 2015. Plants. 2025;14(21):3394-. doi: 10.3390/plants14213394.

4. Wang R, Gamon JA, Hogan KFE, Kellar PR, Wedin DA. Prairie management practices influence biodiversity, productivity and surface-atmosphere feedbacks. The New phytologist. 2025;247(2):562-76. doi: 10.1111/nph.70195.

5. Li M, Wang J, Li K, Liu Y, Ochir A, Davaasuren D. Assessment of grazing livestock balance on the Eastern Mongolian Plateau based on remote sensing monitoring and grassland carrying capacity evaluation. Scientific Reports. 2024;14(1):32151-. doi: 10.1038/s41598-024-84215-4.

6. Hou Q, Ji Z, Yang H, Yu X. Impacts of climate change and human activities on different degraded grassland based on NDVI. Scientific Reports. 2022;12(1):15918.

7. Mu SJ, Chen YZ, Li JL, Ju WM, Odeh IOA, Zou XL. Grassland dynamics in response to climate change and human activities in Inner Mongolia, China between 1985 and 2009. . The Rangeland Journal. 2013;35(3):315-29.

8. Jindo K, Oenema J, Miyoshi Y, Sijbrandij F, Maestrini B, Hoving I, et al. Unlocking the synergistic potential of sensor technologies in grassland research. Discover Sensors. 2025;1(1):19-. doi: 10.1007/s44397-025-00020-2.

9. Liu M, Qu Y, Wang J, Liao Y, Zheng G, Guo Y, et al. A 30-m annual grassland dataset from 1991 to 2020 for Inner Mongolia, China. Scientific Data. 2024;11(1):1143-. doi: 10.1038/s41597-024-03990-x.

10. Xu Z, Sun B, Zhang W, Gao Z, Yue W, Wang H, et al. Is Spectral Unmixing Model or Nonlinear Statistical Model More Suitable for Shrub Coverage Estimation in Shrub-Encroached Grasslands Based on Earth Observation Data? A Case Study in Xilingol Grassland, China. Remote Sensing. 2023;15(23). doi: 10.3390/rs15235488.

11. Chen C, He G, Fang H, Shi L, Zhuang Y, Ding Z, et al. A study on the remote sensing estimation and spatiotemporal distribution patterns of aboveground biomass in savanna grasslands of the Yuanmou dry-hot valley. Frontiers in Plant Science. 2025;16:1648539-. doi: 10.3389/fpls.2025.1648539.

This manuscript is a preprint and has not been peer reviewed. The copyright holder has made the manuscript available under a Creative Commons Attribution 4.0 International (CC BY) license and consented to have it forwarded to EarthArXiv for public posting.

12. Zhenjiang W, Jiahua Z, Fan D, Sha Z, Da Z, Lan X, et al. Fusion of GF and MODIS Data for Regional-Scale Grassland Community Classification with EVI2 Time-Series and Phenological Features. Remote Sensing. 2021;13(5):835-. doi: 10.3390/rs13050835.

13. Zhiwei L, Jianjun Z, Haiqiang F, Cui Z, Tingying Z. Evaluation of the Vertical Accuracy of Open Global DEMs over Steep Terrain Regions Using ICESat Data: A Case Study over Hunan Province, China. Sensors. 2020;20(17):4865-. doi: 10.3390/s20174865.

14. Sun B, Qin P, Li C, Gao Z, Grainger A, Li X, et al. Integrating vegetation phenological characteristics and polarization features with object-oriented techniques for grassland type identification. Geo-Spatial Information Science. 2024;27(3):794-810.

15. Péter T, A. BL, Johannes K, Jodi P, Béla T. The present and future of grassland restoration. Restoration Ecology. 2021;29. doi: 10.1111/rec.13378.

16. Xingguang Y, Jing L, R. SA, Di Y, Tianyue M, YiTing S, et al. Evaluation of machine learning methods and multi-source remote sensing data combinations to construct forest above-ground biomass models. International Journal of Digital Earth. 2023;16(2):4471-91. doi: 10.1080/17538947.2023.2270459.

17. Yanan L, Weishu G, Xiangyun H, Jianya G. Forest Type Identification with Random Forest Using Sentinel-1A, Sentinel-2A, Multi-Temporal Landsat-8 and DEM Data. Remote Sensing. 2018;10(6):946-. doi: 10.3390/rs10060946.

18. Breiman L. Random Forests. Machine Learning. 2001;45(1):5-32. doi: 10.1023/a:1010933404324.

19. Han H, Yin Y, Zhao Y, Qin F. Spatiotemporal Variations in Fractional Vegetation Cover and Their Responses to Climatic Changes on the Qinghai–Tibet Plateau. Remote Sensing. 2023;15(10):2662.

20. Hua L, Xuejian L, Fangjie M, Meng Z, Di'en Z, Shaobai H, et al. Spatiotemporal Evolution of Fractional Vegetation Cover and Its Response to Climate Change Based on MODIS Data in the Subtropical Region of China. Remote Sensing. 2021;13(5):913-. doi: 10.3390/rs13050913.

21. Maake R, Mutanga O, Chirima JG, Kganyago M. Determining Optimal SAR Parameters for Quantifying Above-Ground Grass Carbon Stock in Savannah Ecosystems Using a Tree-Based Algorithm. Remote Sensing in Earth Systems Sciences. 2024;8(1):1-13. doi: 10.1007/s41976-024-00170-8.

22. Mukhtar H, Yang Y, Xu M, Wu J, Abbas S, Wei D, et al. Elevation‐dependent vegetation greening and its responses to climate changes in the south slope of the Himalayas. Geophysical Research Letters. 2025;52(4):e2024GL113276.